



139  
545  
THS

**LIBRARY  
Michigan State  
University**

This is to certify that the  
thesis entitled

**MELTWATER STORAGE AND ITS EFFECT ON ICE-  
SURFACE VELOCITY, MATANUSKA GLACIER, ALASKA**

presented by

**Michiel Arij Kramer**

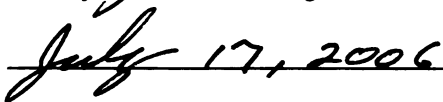
has been accepted towards fulfillment  
of the requirements for the

**Master of  
Science**

degree in

**Department of Geological  
Sciences**

  
Major Professor's Signature

  
Date

**PLACE IN RETURN BOX** to remove this checkout from your record.  
**TO AVOID FINES** return on or before date due.  
**MAY BE RECALLED** with earlier due date if requested.

DATE DUE	DATE DUE	DATE DUE

**MELTWATER STORAGE AND ITS EFFECT ON ICE-SURFACE VELOCITY,  
MATANUSKA GLACIER, ALASKA.**

**By**

**Michiel Arij Kramer**

**A THESIS**

**Submitted to  
Michigan State University  
in partial fulfillment of the requirements  
for the degree of**

**MASTER OF SCIENCE**

**DEPARTMENT OF GEOLOGICAL SCIENCES**

**2006**



## **ABSTRACT**

### **MELTWATER STORAGE AND ITS EFFECT ON ICE-SURFACE VELOCITY, MATANUSKA GLACIER, ALASKA.**

**By**

**Michiel Arij Kramer**

**A surface-energy balance model was constructed for the Matanuska Glacier, south central Alaska, for the 1996 and 1997 ablation seasons. The model calculated shortwave, longwave, sensible and latent energy fluxes across the glacier surface for 5423 cells (250 x 250 m) as well as resultant melt. Results of the model show that shortwave energy was the dominant energy source for melting and that the other three fluxes were small and mostly negative. Comparison of meltwater storage derived from modeled melt and measured discharge with ice-surface velocity measurements showed that an increase in meltwater storage is followed by an increase in ice-surface velocity early in the ablation season.**

## **ACKNOWLEDGEMENTS**

This research was accomplished with the support of many colleagues, friends and members of my family. First and foremost I would like to thank my advisor, Grahame J. Larson. It has been more than a pleasure to work with him on this research and many other projects in Alaska, Iceland and Michigan. The exceptional instruction I received fueled my interest in glacial geology and science in general and encouraged me to continue my career by pursuing a PhD. Second, I would like to thank my committee members, David T. Long and Phanikumar S. Mantha for taking time to critique my thesis and suggesting appropriate changes. Third, I would like to thank Ben W. Brock and Neil S. Arnold for providing me with the original surface-energy balance model and Staci Goetz and Sarah Kopczynski for providing me with necessary data. Fourth, I would like to thank all the people I have worked with in Alaska, especially Dan Lawson, Ed Evenson and Nelson Ham. I would also like to thank some good friends that made my three years in East Lansing a fantastic experience; thank you, Joel, Dave, Nick, Steve and John.

Last but not least I would like to thank my parents, Cobi and Laurens Kramer, for their endless support during my stay in the U. S. and I would like to thank my brother, Erik, for his constant help and encouragement while pursuing my dreams and moving to the U.S.

# TABLE OF CONTENT

LIST OF TABLES.....	VI
LIST OF FIGURES .....	VII
INTRODUCTION .....	1
STUDY AREA.....	3
Ablation .....	6
Ice-surface velocity .....	7
Meltwater discharge .....	8
METHODOLOGY.....	10
Meltwater production .....	10
Matanuska weather station input parameters.....	11
Weather during a sunny summer day .....	12
Net shortwave energy flux.....	12
Albedo of the glacier surface.....	14
Net longwave energy flux .....	16
Turbulent energy fluxes.....	18
Energy transfer by precipitation.....	21
Total melting.....	21
Description of DEM .....	21
Shadow .....	22
SENSITIVITY-ANALYSES.....	23
Albedo .....	23
Shadow .....	24
Temperature.....	25
Temperature lapse rate .....	26
Winter chill layer.....	28
Wind speed .....	29
Aerodynamic surface roughness coefficient.....	31
Calibration .....	32
RESULTS .....	33
Results for cell at the snout and at the accumulation zone .....	33
Results for entire glacier for 1996 and 1997 ablation season.....	35
Shortwave energy flux.....	37
Longwave energy flux .....	38
Sensible energy flux.....	38
Latent energy flux.....	39
Total energy flux.....	39

DISCUSSION.....	40
Modeled melt and measured discharge .....	40
Measured discharge and ice-surface velocity .....	43
Meltwater storage and ice-surface velocity .....	45
CONCLUSIONS.....	49
General conclusion .....	50
REFERENCES .....	51

## LIST OF TABLES

Table 1.	Surface-energy balance model results in $W\ m^{-2}$ : average, minimum and maximum shortwave, longwave, sensible and latent energy for day 140 to 213 (May 19 to July 31), 1996. ....	35
Table 2.	Surface-energy balance model results in $W\ m^{-2}$ : average, minimum and maximum shortwave, longwave, sensible and latent energy for day 94 to 234 (April 4 to August 22), 1997. ....	36

# LIST OF FIGURES

(Images in this thesis are presented in color)

Figure 1.	Location map for the Matanuska Glacier, Alaska (modified from Waterson, 2003).	3
Figure 2.	Hypsometric curve (altitudinal distribution) for the Matanuska Glacier.	4
Figure 3.	Winter temperature profile, March 1999, Matanuska Glacier.	6
Figure 4.	Ice-surface velocity Matanuska Glacier for 1996 and 1997 ablation seasons (Ensminger, 1999) (Velocity derived from 7-point moving average of the average of multiple target stations near the snout of the glacier.)	7
Figure 5.	Measured daily discharge South Branch, Matanuska Glacier for the 1996 and 1997 ablation seasons (Linker, 2001 and Waterson, 2003)	9
Figure 6.	Shortwave energy for the Matanuska Glacier with different albedo values for the 1996 ablation season.	24
Figure 7.	Longwave and sensible energy for the Matanuska Glacier with different temperature for the 1996 ablation season.	25
Figure 8.	Longwave energy using different temperature lapse rates for the 1996 ablation season.	26
Figure 9.	Sensible energy using different temperature lapse rates for the 1996 ablation season.	27
Figure 10.	Latent energy using different temperature lapse rates for the 1996 ablation season.	28
Figure 11.	Effect of substituting measured wind speed with $0.01 \text{ m s}^{-1}$ and $5.0 \text{ m s}^{-1}$ on sensible energy for the 1996 ablation season.	30
Figure 12.	Effect of substituting measured wind speed with $0.01 \text{ m s}^{-1}$ and $5.0 \text{ m s}^{-1}$ on latent energy for the 1996 ablation season.	30
Figure 13.	Sensible and latent energy for the Matanuska Glacier with different aerodynamic surface roughness coefficients for day 140 to 150, 1996.	31

Figure 14. Cumulative modeled melt versus cumulative measured ablation for day 150 to 213, 1996.....	32
Figure 15. Shortwave, longwave, sensible and latent energy for a cell at the snout of the glacier at day 173, 1996.....	33
Figure 16. Shortwave, longwave, sensible and latent energy for a cell at the accumulation zone of the glacier at day 173, 1996. ....	34
Figure 17. Surface-energy balance model results for the 1996 ablation season.....	36
Figure 18. Surface-energy balance model results for the 1997 ablation season.....	37
Figure 19. Modeled melt and measured discharge for the 1996 ablation season.....	42
Figure 20. Modeled melt and measured discharge for the 1997 ablation season.....	43
Figure 21. Measured discharge and ice-surface velocity for the 1996 ablation season.....	44
Figure 22. Measured discharge and ice-surface velocity for the 1997 ablation season.....	45
Figure 23. Meltwater storage and ice-surface velocity for the 1996 ablation season.....	47
Figure 24. Meltwater storage and ice-surface velocity for the 1997 ablation season.....	48

# **INTRODUCTION**

Meltwater derived from surface melting commonly tends to follow different paths through a temperate glacier and ultimately will drain via meltwater channels at the glacier margin. During this process some meltwater is temporarily stored within and under the ice (Jansson et al., 2003).

Several studies (Iken, 1981; Iken et al., 1983; Iken and Bindshadler, 1986; Iken and Truffer, 1997; Ensminger et al, 1999; Jansson et al, 2003) have suggested that variations in ice-surface velocities are related to variations in meltwater storage within the subglacial drainage system and that increasing ice-surface velocities are related to increasing storage at the glacier bed, while decreasing velocities are related to release of stored water.

In order to test the relationship between ice-surface velocities and meltwater storage, detailed information on the amount of glacial meltwater being stored within the glacier is crucial. Since it is physically very difficult to measure storage under and within a glacier it has been inferred in all studies by measuring related parameters. For example, use of basal water pressure as an indication of the amount of storage has been used by Iken & Bindshadler (1986), Willis (1992) and (Harper, 2005). Other approaches have used meltwater input as an indicator for subglacial storage and related this to ice-surface velocity (Yamaguchi, 2003) or related the amount of discharge to ice velocity (Naruse, 1992, Raymond, 1995). Some studies have used a deficit in runoff in a water balance study to calculate storage (Hodgkins, 2001; Schuler et al. 2002; Singh,



2003, Matsumoto, 2004), but fail to directly relate calculated storage to ice-surface velocities.

This research focuses on calculation of storage at the Matanuska Glacier in south-central Alaska using a deficit in run-off and tests the hypothesis that an increase in meltwater storage results in an increase in ice-surface velocity.

## STUDY AREA

The Matanuska Glacier (Figure 1) is a large temperate valley glacier originating in ice fields in the Chugach Mountains, south-central Alaska, and flows north into the Matanuska valley. It is approximately 45 km long and ranges in width from 3 km near the equilibrium line to about 5 km near the terminus.

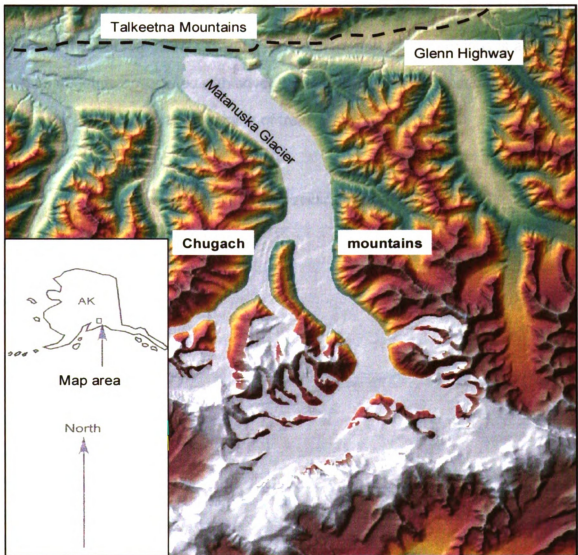
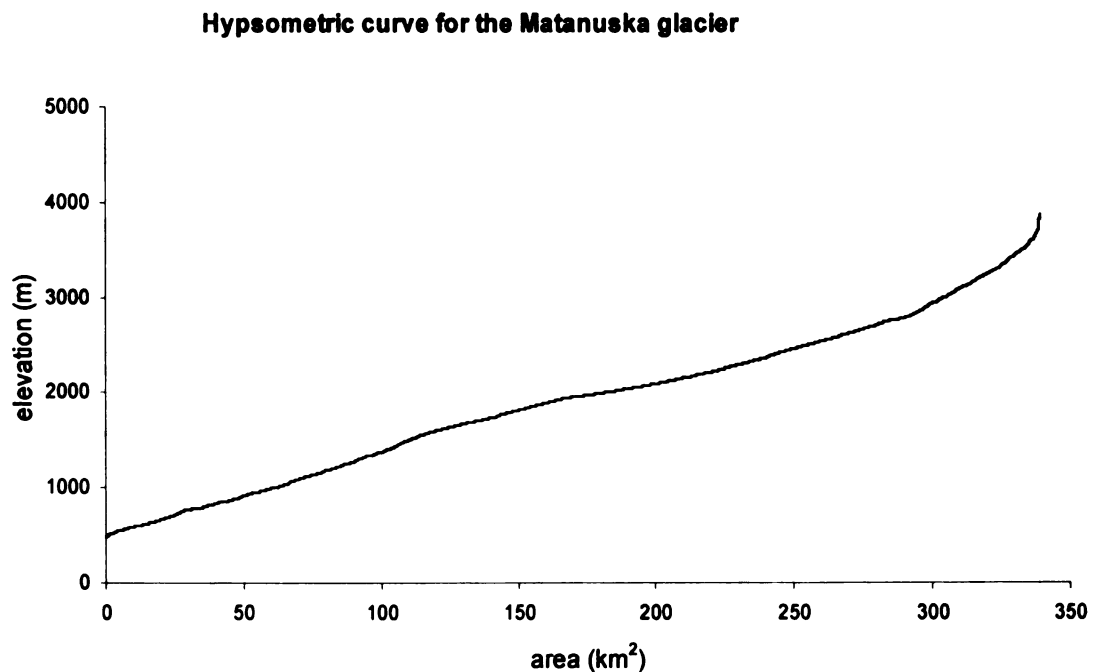


Figure 1. Location map for the Matanuska Glacier, Alaska (modified from Waterson, 2003).

The glacier covers about 341 km<sup>2</sup> or 56% of a drainage basin that is about 612 km<sup>2</sup>. Elevation of the glacier surface (Figure 2) ranges from about 3800 m at its highest point near Mount Marcus Baker to about 500 m at its terminus (Lawson et al., 1998b).

The glacier terminus has been at a relatively stable position for the last 200 years (Williams and Ferrins, 1961), however, unpublished data Lawson (personal communication, 2003) suggests the terminus has retreated 10 to 30 m yr<sup>-1</sup> over the last ten years. Covering the northern part of the terminus is a broad mantle of debris associated with several medial moraines. In places the debris is > 1 m thick and supports the growth of trees and shrubs.



**Figure 2.** *Hypsometric curve (altitudinal distribution) for the Matanuska Glacier.*

An automated weather station has been maintained during the summers by the U.S. Army Cold Regions Research and Engineering Laboratory since 1994 and is located 200 m beyond the ice margin. This station records incoming shortwave radiation, reflected shortwave radiation, longwave energy, air temperature, wind speed, wind direction, relative humidity and precipitation.

The nearest continuously recording weather station to the Matanuska Glacier is located at Sheep Mountain Airstrip which lies approximately 15 km west of the glacier terminus at an elevation of 850 m. Temperature records from 1961 to 1990 for this station show a monthly mean minimum temperature of -20 °C and a monthly mean maximum of 17 °C with a mean annual minimum of -7.05 °C and a mean annual maximum of 2.6 °C. Annual precipitation records from year 1961 to 1990 show a mean total precipitation of 366 mm (Western Regional Climate Center). In general, summers at the Matanuska Glacier are sunny, interrupted occasionally by cloudy days (2-3) with some light drizzle. Rarely are there days of heavy rainfall.

A thermistor string installed in a 30 m deep borehole drilled into the snout of the glacier by CRREL in 1999 revealed that winter air temperatures chill the top layer of the glacier to a depth of about 12 m and to a minimum temperature of nearly -8°C (Figure 3).

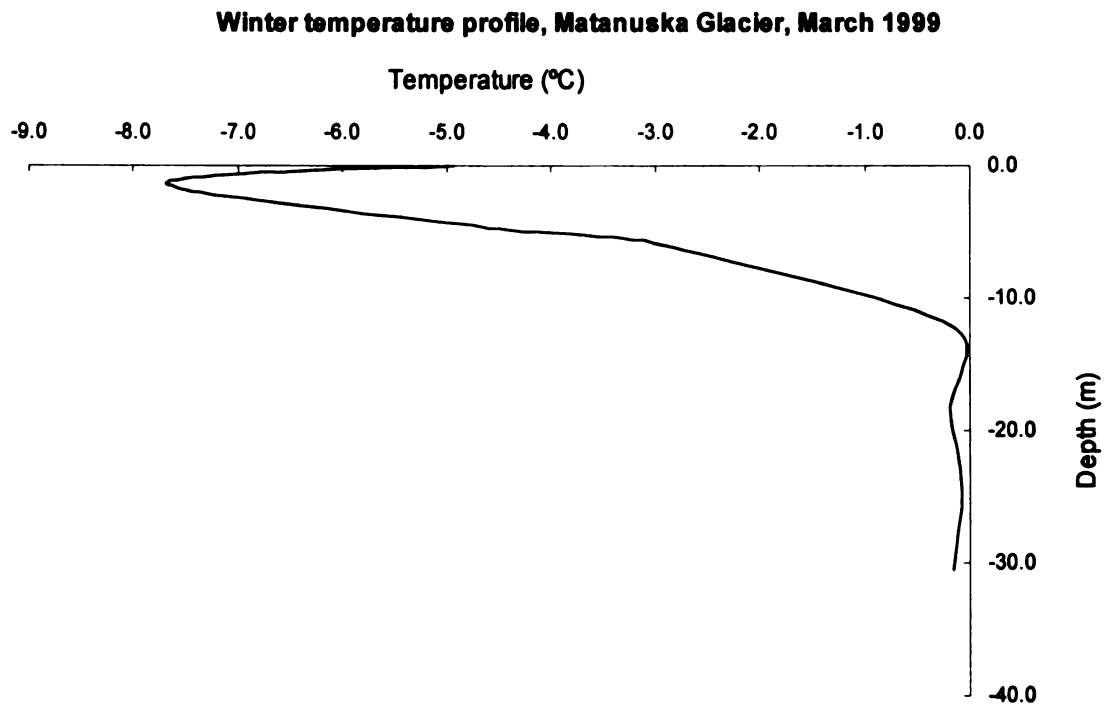


*Figure 3. Winter temperature profile, March 1999, Matanuska Glacier.*

## **Ablation**

Daily ablation measurements were made at the western terminus of the Matanuska Glacier during the 1996 and 1997 ablation seasons using white PVC stakes drilled into the ice surface. Daily records of ablation were obtained by measuring from the top of the stake down to the ice surface. Average daily ablation for 1996 was  $4.3 \text{ cm day}^{-1}$ , with a minimum of  $0.1 \text{ cm day}^{-1}$  and a maximum of  $8.9 \text{ cm day}^{-1}$ . In 1997, average daily ablation was  $8.8 \text{ cm day}^{-1}$  and the minimum was  $1.8 \text{ cm day}^{-1}$  and the maximum was  $18.5 \text{ cm day}^{-1}$ .

## Ice-surface velocity

Ice-surface velocity has been measured at the Matanuska Glacier during the 1996 and 1997 ablation seasons (Ensminger et al., 1999) and is presented in Figure 4. The measurements generally show variations in ice-surface velocity throughout the two ablation seasons. The average velocity for 1996 was 16.65  $\text{cm day}^{-1}$ , with a maximum of 27.89  $\text{cm day}^{-1}$  and a minimum of 8.89  $\text{cm day}^{-1}$ . In 1997, average velocity was 16.25  $\text{cm day}^{-1}$  and the maximum was 34.28  $\text{cm day}^{-1}$  and the minimum was 9.55  $\text{cm day}^{-1}$ .

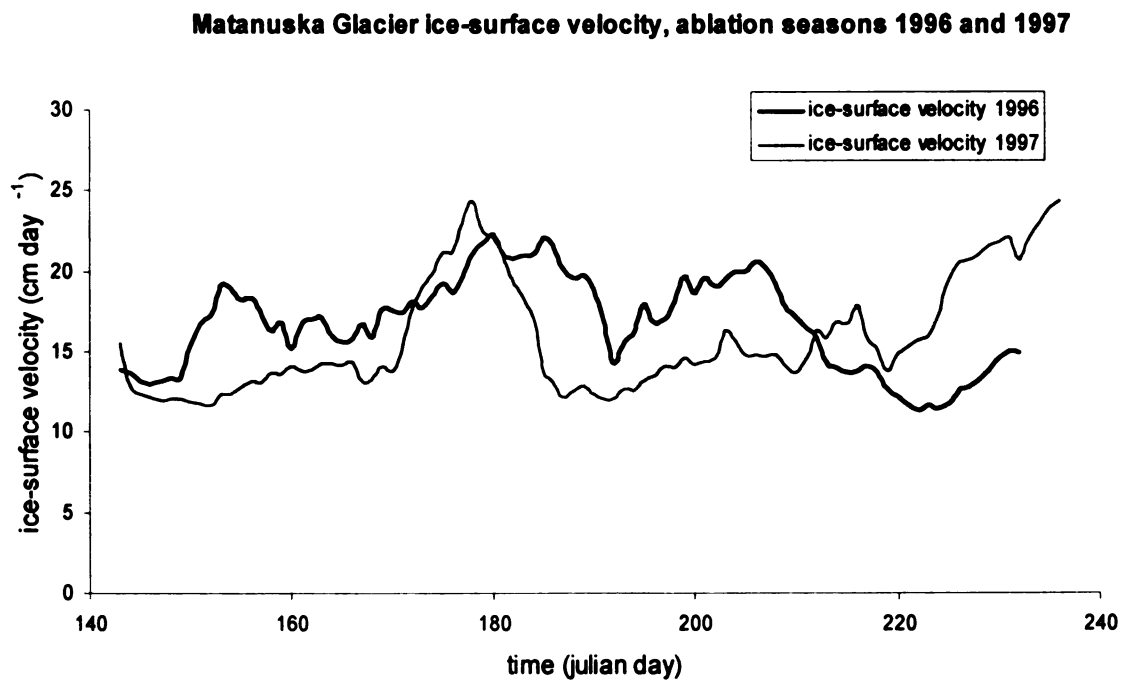


**Figure 4.** *Ice-surface velocity Matanuska Glacier for 1996 and 1997 ablation seasons (Ensminger, 1999) (Velocity derived from 7-point moving average of the average of multiple target stations near the snout of the glacier.)*

## **Meltwater discharge**

The drainage system of the Matanuska Glacier is generally characterized by a complex network of subglacial conduits feeding discharge vents at the glacier margin (Lawson et al., 1998b). In turn, these vents feed three main meltwater streams draining the glacier, North Branch, South Branch and Little River. Since 1995, the U.S. Army Cold Regions Research and Engineering Laboratory (CRREL) has maintained gauging stations on the meltwater streams that record discharge in intervals of ten minutes.

For the summer season of 1996 discharge recorded in South Branch (Figure 5) constituted 94% of the discharge recorded in the three streams draining the glacier (Linker, 2001). Discharge in South Branch was minimal around Julian day 165 after which it rapidly increased to a peak discharge of  $7.76\text{E}+06 \text{ m}^3 \text{ day}^{-1}$  at day 188. Discharge then declined to  $4.74\text{E}+06 \text{ m}^3 \text{ day}^{-1}$  on day 197 after which it increased again to a slightly higher second discharge peak of  $8.32\text{E}+06 \text{ m}^3 \text{ day}^{-1}$  at day 205. Discharge then decreased, to  $3.17\text{E}+06 \text{ m}^3 \text{ day}^{-1}$  at day 223 and once more increased to a third somewhat subdued discharge peak, of  $5.59\text{E}+06 \text{ m}^3 \text{ day}^{-1}$  at day 232. Following the third discharge peak, discharge steadily decreased to  $2.67\text{E}+06 \text{ m}^3 \text{ day}^{-1}$  by day 274. Average discharge over the measured ablation period was  $4.02\text{E}+06 \text{ m}^3 \text{ day}^{-1}$ .

For the summer of 1997 discharge recorded in South Branch (Figure 5) also constituted 94% of the discharge recorded in the three streams draining the glacier (Linker, 2001) and showed a pattern similar to that of 1996. Discharge was minimal until day 169, after which it rapidly increased to a peak of

1.31E+07 m<sup>3</sup> day<sup>-1</sup> at day 182. Discharge then decreased to 7.32E+06 m<sup>3</sup> day<sup>-1</sup> by day 203, and then increased again to a slightly lower peak of 1.29E+07 m<sup>3</sup> day<sup>-1</sup> by day 211. Discharge then decreased to 8.08E+06 m<sup>3</sup> day<sup>-1</sup> at day 221 and once more increased to the third discharge peak 1.28E+07 m<sup>3</sup> day<sup>-1</sup> by day 225. Following the third peak discharge decreased to 5.84E+06 m<sup>3</sup> day<sup>-1</sup> by day 236. Average discharge over the measured summer period in 1997 was 8.02E+06 m<sup>3</sup> day<sup>-1</sup>, about twice as much as the previous year.

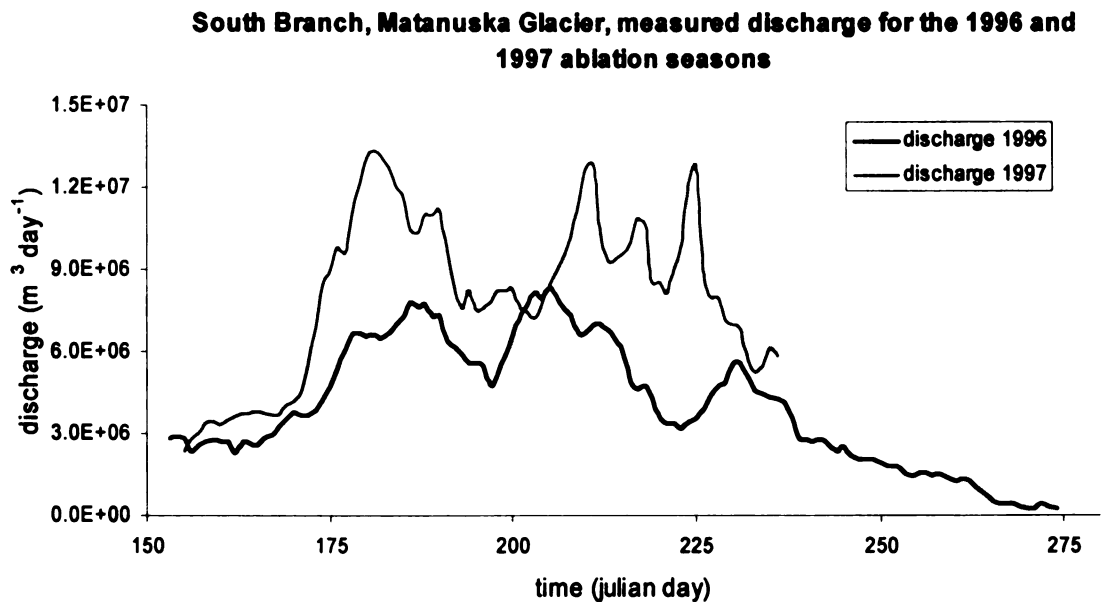


**Figure 5.** *Measured daily discharge South Branch, Matanuska Glacier for the 1996 and 1997 ablation seasons (Linker, 2001 and Waterson, 2003)*



## METHODOLOGY

### Meltwater production

Meltwater production at the Matanuska Glacier was calculated for May 19<sup>th</sup> to August 1<sup>st</sup> 1996 (Julian day 140 to 214) and for April 4<sup>th</sup> to August 22<sup>nd</sup> (day 94 to 234) 1997 using an adjusted point surface-energy balance model, originally developed by Brock and Arnold (2000). This model is constructed around the general surface-energy balance equation:

$$Q_m = Q_{rs} \pm Q_{rl} \pm Q_s \pm Q_i + Q_p \quad (1)$$

where,

$Q_m$ = total energy for melting

$Q_{rs}$ = net shortwave energy flux

$Q_{rl}$ = net longwave energy flux

$Q_s$ = net sensible energy flux

$Q_i$ = net latent energy flux

$Q_p$ = heat transfer by precipitation

The model calculates net shortwave and longwave energy fluxes, turbulent sensible and latent energy fluxes and surface melting rate at a point in time for 5423 cells (250 by 250 m) representing the glacier surface. A positive flux means a transfer of energy into the glacier, i.e. the glacier surface warms up and can the ice can melt, whereas negative fluxes release energy from the

glacier, i.e. the glacier cools. Calculations were made from hourly inputs of incoming shortwave energy, vapor pressure, air temperature and wind speed, all of which were obtained from the glacier weather station. Also used in the calculations were latitude, longitude, slope angle, aspect and elevation, which were obtained from a Digital Elevation Model (DEM) of the glacier. Other parameters specified in the model were local temperature lapse rate, ice-surface aerodynamic roughness, ice-surface albedo and elevation of the weather station (Brock and Arnold, 2000).

The output of the surface-energy balance model includes hourly and daily rates of net shortwave and longwave-energy fluxes, turbulent and latent-energy fluxes and surface-melt. The energy fluxes can be expressed in terms of equivalent amount of water melted (mm), which was obtained by dividing the total energy flux by latent heat of fusion of water (Brock and Arnold, 2000).

### **Matanuska weather station input parameters**

Based on the Matanuska weather station maximum shortwave energy values for a typical summer occur around the third week of June and can be as high as  $800 \text{ W m}^{-2}$ ; mean daily value of shortwave energy over a typical summer is  $236 \text{ W m}^{-2}$ . Mean air vapor pressure is about 788 Pa with maximum around 1200 Pa and minimum as low as 230 Pa. Mean air temperature over the summer is  $10^{\circ}\text{C}$ , with a minimum air temperature of  $0^{\circ}\text{C}$  (beginning of May) and a maximum temperature just above  $20^{\circ}\text{C}$ . Average precipitation is  $0.54 \text{ mm day}^{-1}$

with a maximum of  $7.79 \text{ mm day}^{-1}$ ; total precipitation over the summer of 1996 is 48.82 mm.

Mean wind speed over a typical summer is about  $2.0 \text{ m s}^{-1}$  with maxima around  $6.0 \text{ m s}^{-1}$ . General wind direction is from the east-southeast, caused by katabatic winds blowing down glacier.

### **Weather during a sunny summer day**

During a typical sunny summer day on the glacier the lowest temperature, generally around  $6^{\circ}\text{C}$ , is in the morning, rising to a maximum of about  $20^{\circ}\text{C}$  in the late afternoon. Typical wind-speed patterns follow temperature, low wind speed ( $0.5 \text{ m s}^{-1}$ ) in the morning, increasing to a maximum wind speed ( $4.5 \text{ m s}^{-1}$ ) in the late afternoon or early evening.

### **Net shortwave energy flux**

Net shortwave energy was calculated following the method as described by Brock and Arnold (2000). The method involves measuring incoming shortwave energy ( $Q_{\text{in}}$ ) in a horizontal plane at the glacier meteorological station and assumes that incoming shortwave energy measured is representative for all points on the glacier surface (Brock and Arnold, 2000). However, in this study the effect of shadow also was calculated for every cell.

Solar elevation and azimuth were calculated using cell latitude and longitude, solar day and hour.  $Q_{\text{in}}$  was split into its direct ( $Q_{\text{dir}}$ ) and diffuse ( $Q_{\text{dif}}$ )

components using an estimate of cloud cover obtained by comparing the measured incoming shortwave energy ( $Q'$ ) with theoretical maximum incoming shortwave energy ( $K$ ) (Brock and Arnold, 2000).  $K$  was calculated using:

$$K = I_0 \psi \left( \frac{P}{P_0} \right) \cos \theta \quad (2)$$

where,  $I_0$  is the solar constant ( $1368 \text{ W m}^{-2}$ ),  $\psi$  is the atmospheric clear-sky transmissivity (0.75),  $P$  is the atmospheric pressure,  $P_0$  is the mean atmospheric pressure at sea level (assumed to be constant at 100,000 Pa) and  $\theta$  is the solar zenith angle (Oke, 1987; Hock and Noetzli, 1997). When the ratio of measured incoming shortwave energy ( $Q'$ ) and theoretical maximum incoming shortwave energy ( $K$ ) is 1, there is no cloud cover ( $n=0.0$ ). With a decrease in the ratio  $Q':K$  there is a linear increase in  $n$ . For  $Q':K$  ratios  $\leq 0.2$  cloud cover is assumed to be 1.0 (Brock and Arnold, 2000). At night a cloud cover of 0.25 is assumed.

After calculating cloud cover the diffuse fraction ( $D_f$ ) of total incoming shortwave energy was calculated from:

$$D_f = (0.65n + 0.15) \quad (3)$$

Energy from direct incoming shortwave energy was then calculated as:

$$Q_{\text{dir}} = (1 - D_f) Q' n [\sin Z \cos Z' + \cos Z \sin Z' \cos(A - A')] \quad (4)$$

and energy from diffuse incoming shortwave energy was calculated as:

$$Q_{dif} = D_f Q' \cos^2(Z' / 2) + \alpha Q' \sin^2(Z' / 2) \quad (5)$$

where,  $Z'$  is the angle of the slope from the horizontal,  $A$  is solar azimuth,  $A'$  is slope aspect,  $\alpha$  is glacier surface albedo.

Finally, the net shortwave energy flux was calculated using:

$$Q_{rs} = (1 - \alpha)Q_{dir} + (1 - \alpha)Q_{dif} \quad (6)$$

where,  $\alpha$  is glacier surface albedo.

### **Albedo of the glacier surface**

Approximately 40 spot albedo measurements were made at the Matanuska Glacier during the 2004 ablation season using a Kipp & Zonen Cm 14b albedometer (serial number: 980119), which is constructed around two Cm 11 pyranometers. Data from the 2004 ablation season was assumed to be representative for the albedo during the summers of 1996 and 1997. Using a hand held mounting rod and bubble level horizontal measurements were made about 1 m above mainly horizontal glacier surfaces around noon. Incoming shortwave energy and reflecting shortwave energy were recorded, with the ratio of the two yielding the albedo value. Albedo values range from < 10% above

debris-covered ice at the snout of the glacier to 64% above relatively old melting snow in the accumulation zone.

In addition, broadband 3 (range 0.3-5.0  $\mu\text{m}$ ) spectrum of the MODIS Terra Albedo 16-day L3 Global 1km SIN GRID V004 product was used to estimate surface albedo since 99% of shortwave radiation at the earth's surface is from 0.3 to 3.0  $\mu\text{m}$ . MODIS data for years 1996 and 1997, however, was not available and therefore data from the summer of 2003 was selected and assumed to be representative for the distribution of albedo during the summers of 1996 and 1997. Albedo values above 50% were considered to be snow-covered and were used to estimate snowline elevation for Julian days 113, 161, 177, and 195. A best-fit logarithmic curve similar to that found by Hannah et. al. (1999) and Tangborn (1999) was then fitted through these elevations, giving a snowline regression function over time:

$$h = 2496.8\text{Ln}(t) - 111019 \quad (7)$$

where,  $h$  is snowline elevation in meters and  $t$  is time in Julian days.

Another function was developed to account for ripening of snow over time. Fresh dry snow can have an albedo value as high as 97%, but melting snow and firn have values typically around 74% and 53%, respectively (Patterson, 1994). For twenty randomly chosen points in the accumulation zone albedo values of snow-covered glacier surface were plotted for Julian day 113, 161, 177, and 195

and a linear curve was fitted through these points, giving a function representing a decline in albedo over time.

$$\alpha = \alpha - 0.0014 * t \quad (8)$$

where,  $\alpha$  is the surface albedo and  $t$  is time in Julian days.

Using the MODIS product two albedo maps also were generated. One was representative for the beginning of the ablation season with most of the glacier surface snow covered, the snow-albedo map, and the other for the end of the ablation season with most of the glacier ice exposed, the ice-albedo map.

The elevation of the snowline at a specific day for the Matanuska Glacier was calculated using the snowline regression function. If the point of interest was located below the snowline, glacier ice was exposed and the point of interest was assigned the albedo value from the ice-albedo map. If the point of interest was located above the snowline, the surface was covered with snow and the albedo value was assigned from the snow-albedo map, adjusted for the riping effect using the snow-ripping function.

### **Net longwave energy flux**

Assuming the glacier is 0°C and radiates as a black body, outgoing longwave energy ( $I_{out}$ ) was calculated using the Stefan-Boltzmann Law (Oke, 1987 and Patterson, 1994.):

$$I_{out} = \sigma T^4 \quad (9)$$

where, T is the absolute temperature (0°C or 273.15K) and  $\sigma$  is the Stefan's constant ( $5.67 \times 10^{-8} \text{ W m}^{-2} \text{ K}^{-4}$ ) resulting in  $I_{out}=316 \text{ W m}^{-2}$ . Incoming longwave energy ( $I_{in}$ ) was calculated, again using the Stefan-Boltzmann Law:

$$I_{in} = \epsilon^* \sigma T_a^4 \quad (10)$$

where,  $\epsilon^*$  is the effective emissivity of the sky, calculated following Arnold *et al.* (1996):

$$\epsilon^* = (1 + \kappa n) \epsilon_0 \quad (11)$$

where n is the amount of cloud cover, and  $\epsilon_0$  is the clear-sky emissivity ( $8.733 \times 10^{-3} T_a^{0.788}$ ) and  $\kappa$  is a constant depending on cloud type. Chosen was a value of 0.26, the mean value for altostratus, stratocumulus, stratus and cumulus cloud types (Braithwaite and Olesen, 1990). Finally, longwave energy flux was calculated using:

$$Q_{rl} = I_{in} - I_{out} \quad (12)$$



## Turbulent energy fluxes

Since only wind speed and temperature data at one height above the ground surface was available from the glacier meteorological station the bulk aerodynamic method was used to calculate the turbulent energy fluxes, sensible energy flux ( $Q_s$ ) (lost or gained by conductance and turbulence) and latent energy flux ( $Q_i$ ) (lost or gained due to condensation and evaporation) at the glacier surface (Munro 1989, 1990).

$$Q_s = \frac{\rho \omega \lambda k^2 u_z (e_z - e_s) / P}{\left[ \ln\left(\frac{z}{z_0}\right) + \frac{a_M z}{\Lambda} \right] \left[ \ln\left(\frac{z}{z_e}\right) + \frac{a_E z}{\Lambda} \right]} \quad (13)$$

$$Q_i = \frac{\rho c_p k^2 u_z T_z}{\left[ \ln\left(\frac{z}{z_0}\right) + \frac{a_M z}{\Lambda} \right] \left[ \ln\left(\frac{z}{z_e}\right) + \frac{a_E z}{\Lambda} \right]} \quad (14)$$

where:

$u_z$  = wind speed ( $\text{m s}^{-1}$ )

$T_z$  = temperature ( $^{\circ}\text{C}$ )

$e_z$  = vapor pressure (Pa) at height  $z(\text{m})$

$e_s$  = vapor pressure at glacier surface, assumed to be 611 Pa above a melting ice surface (Oke, 1987).

$c_p$  = specific heat of air at constant pressure ( $\text{J kg}^{-1} \text{K}^{-1}$ ), calculated as  $1004.67 * (1 + 0.84 * \text{specific humidity})$

$\rho$  = air density,  $1.26 \text{ kg m}^{-3}$  for low positive air temperatures

$\kappa$  = von Kármán's constant, 0.40 (Oke, 1987)

$\omega$  = ratio of molecular weight of water vapor to air, 0.622

$\lambda$  = latent heat of vaporization,  $2.5 \times 10^6 \text{ J kg}^{-1}$  at  $0^\circ\text{C}$

$a_M$ ,  $a_H$  and  $a_E$  : stability corrections for momentum, heat and humidity, respectively. Assumed to be 5 (Inoue, 1989; Munro, 1989, 1990 and Braithwaite 1995).

$\Lambda$ : the Monin-Obukhov length scale (Obukhov, 1971), calculated using:

where:

$$\Lambda = \frac{\rho c_p u_*^3 T_k}{kg Q_i} \quad (15)$$

$T_k$  = the absolute mean temperature (K) of the air in the surface layer between  $z$  and the target cell

$G$  = the gravitational acceleration (9.81)

$u^*$  = frictional velocity, calculated following Munro(1989):

$$u^* = \frac{\kappa u_z}{\left[ \ln\left(\frac{z}{z_0}\right) + a_x \left(\frac{z}{\Lambda}\right) \right]} \quad (16)$$

In order to calculate  $\Lambda$  prior knowledge of  $Q_s$  and  $u^*$  is required, which in turn depends on  $\Lambda$ . Use of a simple iteration loop solves this problem.  $Q_s$  was first evaluated for a neutral surface layer, with  $z/L=0$ , then the first estimate of  $\Lambda$  was made. This result was then used to recalculate  $Q_s$  and  $u^*$  (Munro, 1989). This procedure was repeated until  $\Lambda$  was unchanged which occurred in general after five iterations (Munro 1989). Instead of assuming  $z_0=z_t=z_e$ , the scaling lengths for temperature and humidity were calculated as functions of the aerodynamic roughness length,  $z_0$ , and flow, using the roughness Reynolds number,  $Re^*$  (Andreas, 1987; Munro, 1989):

$$\ln\left(\frac{z_t}{z_0}\right) = 0.317 - 0.565\ln(Re^*) - 0.183\ln(Re^*)^2 \quad (17)$$

$$\ln\left(\frac{z_e}{z_0}\right) = 0.396 - 0.512\ln(Re^*) - 0.180\ln(Re^*)^2 \quad (18)$$

The roughness Reynolds number was calculated as

$$Re^* = u^* \frac{z_0}{\nu} \quad (19)$$

where  $\nu$  is the kinematic viscosity of air ( $1.461 \times 10^{-5} \text{ m}^2\text{s}^{-1}$ ) (Stull, 1988).

## **Energy transfer by precipitation**

Since precipitation for the 1996 and 1997 ablation seasons is generally < 50 mm the energy flux from rain was considered negligible compared to the other energy sources and thus not included in the surface-energy balance model (Brock and Arnold, 2000; Hock and Holmgren, 2005).

## **Total melting**

Surface melting rate was calculated as the sum of the four fluxes and the melting rate was then converted to mm w. e. (water equivalent) by dividing the melting rate by the latent heat of fusion of water ( $0.334 \times 10^6 \text{ J kg}^{-1}$ ).

## **Description of DEM**

The Digital Elevation Model (DEM) used in this research was downloaded from the USGS seamless data website (<http://www.seamless.usgs.gov>). The initial DEM was in GCS North American 1927 projection, with units in degrees and a cell size of 0.00056 x 0.00056 degrees. The projection was changed to NAD 1927 UTM zone 6 North projection with units in meters to produce a new DEM with cell sizes 45.67 x 45.67 meters. This new DEM was then resampled to create a third DEM with cell sizes of 250 x 250 meters that was used to determine the total area of the Matanuska Glacier watershed and generate a slope and aspect map for the glacier.

Also downloaded from the USGS were nine topographic maps covering the Matanuska Glacier. These were used to outline the extent of the glacier and to calculate the total area of the Matanuska Glacier. All of the analyses were performed in ArcGis

## **Shadow**

To evaluate the effect of shadows on the glacier surface a time sensitive analysis of shading was included in the surface-energy balance model. This analysis used latitude, longitude and elevation of the target cell; all derived from the DEM, as well as solar azimuth and solar elevation. Using a bilinear interpolation technique, elevations were calculated along a line from the target cell to the sun. Angles between these elevation points and the target cell were then calculated. If any of the angles were greater than the solar elevation angle, the rays from the sun were considered obstructed and did not reach the target cell, i.e. the target cell was in shade and did not receive shortwave energy.

## **SENSITIVITY-ANALYSES**

### **Albedo**

Modeled shortwave energy for a wide range of published constant albedo values for ice and snow during the 1996 ablation season is presented in Figure 6. The figure shows that modeled shortwave energy based on a constant ice albedo of 0.2 and constant snow albedo of 0.6 was almost identical to that based on MODIS derived albedo values. However, when an ice albedo of 0.3 and a snow albedo of 0.7 was used the modeled melt became lower. This difference became even greater when an ice albedo of 0.4 and snow albedo of 0.8 was used.

In the final surface-energy balance model an albedo value of 0.3 for ice and 0.7 for snow was chosen because the author believes it best represents the ice-surface albedo, based on in-situ measurements as well as average values for snow and ice albedo (Patterson, 1994). Also, MODIS values tend to underestimate albedo because they are derived by an interpolation technique that include albedo values from surrounding, non-glacier surfaces.

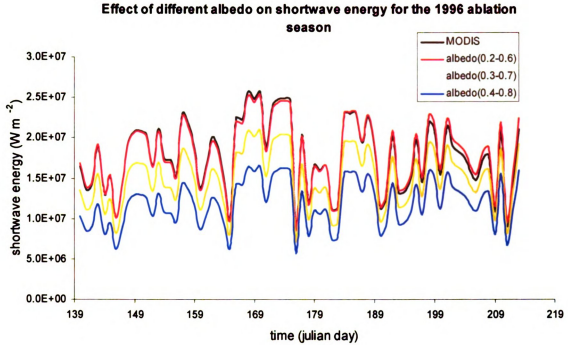


*Figure 6. Shortwave energy for the Matanuska Glacier with different albedo values for the 1996 ablation season.*

## Shadow

The effect of shadow being cast on the glacier surface by the surrounding topography was analyzed and showed only an average 7% decrease of the shortwave energy on the glacier surface. This is due to the fact that solar radiation receipts are low during low sun angles and represent only a small fraction of total shortwave energy received by the glacier throughout the day.

## Temperature

The effect of adding 2°C from temperature recorded at the glacier weather station on both longwave energy and sensible energy flux is presented in Figure 7. The figure shows that both longwave energy and sensible energy fluxes are almost identical with a change of 2°C. For this reason the author believes temperature recorded at the glacier weather station is a reasonable input parameter to the surface-energy balance model.

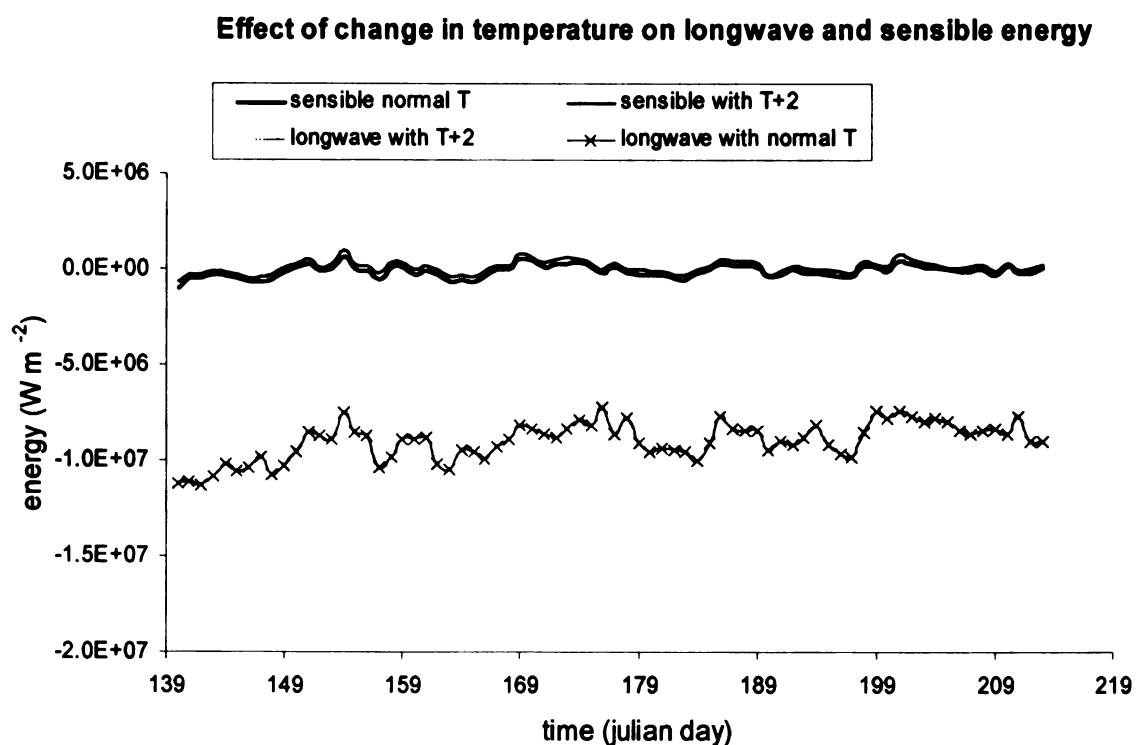


**Figure 7.** Longwave and sensible energy for the Matanuska Glacier with different temperature for the 1996 ablation season.



## Temperature lapse rate

The effect of different temperature lapse rates on longwave, sensible and latent energy fluxes for the 1996 ablation season is presented in Figure 8, 9 and 10. The figures show that changing the temperature lapse rate from  $0.009^{\circ}\text{C m}^{-1}$  to  $0.006^{\circ}\text{C m}^{-1}$  and  $0.012^{\circ}\text{C m}^{-1}$  does affect the different individual energy fluxes, but not enough to appreciable affect the total energy balance.

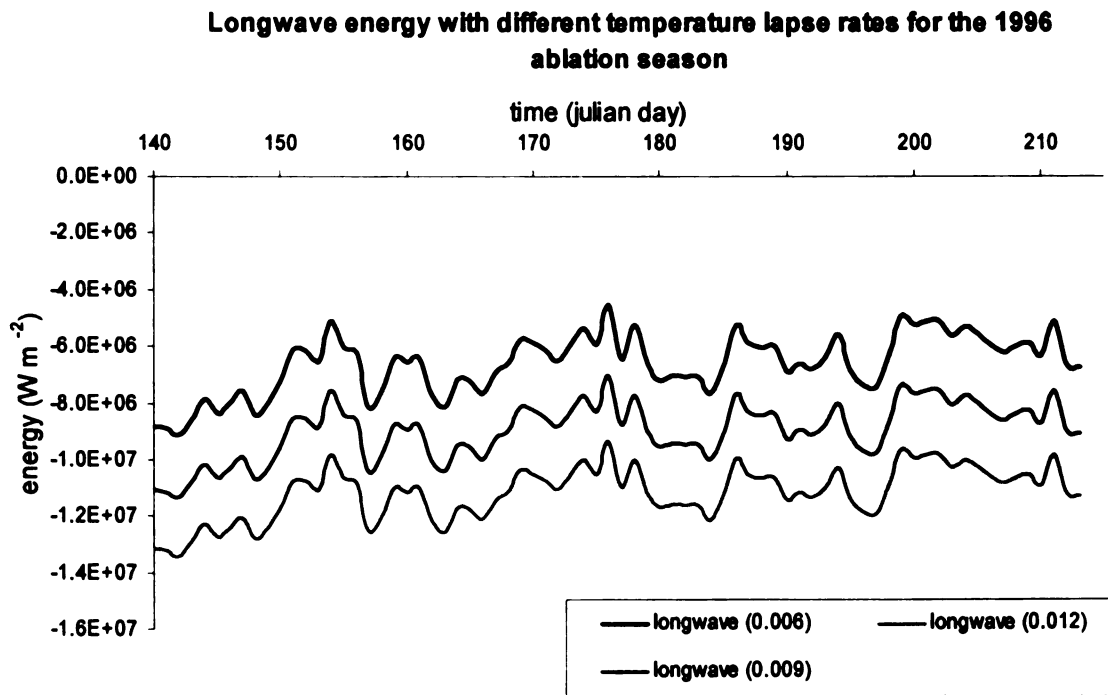


**Figure 8.** Longwave energy using different temperature lapse rates for the 1996 ablation season.

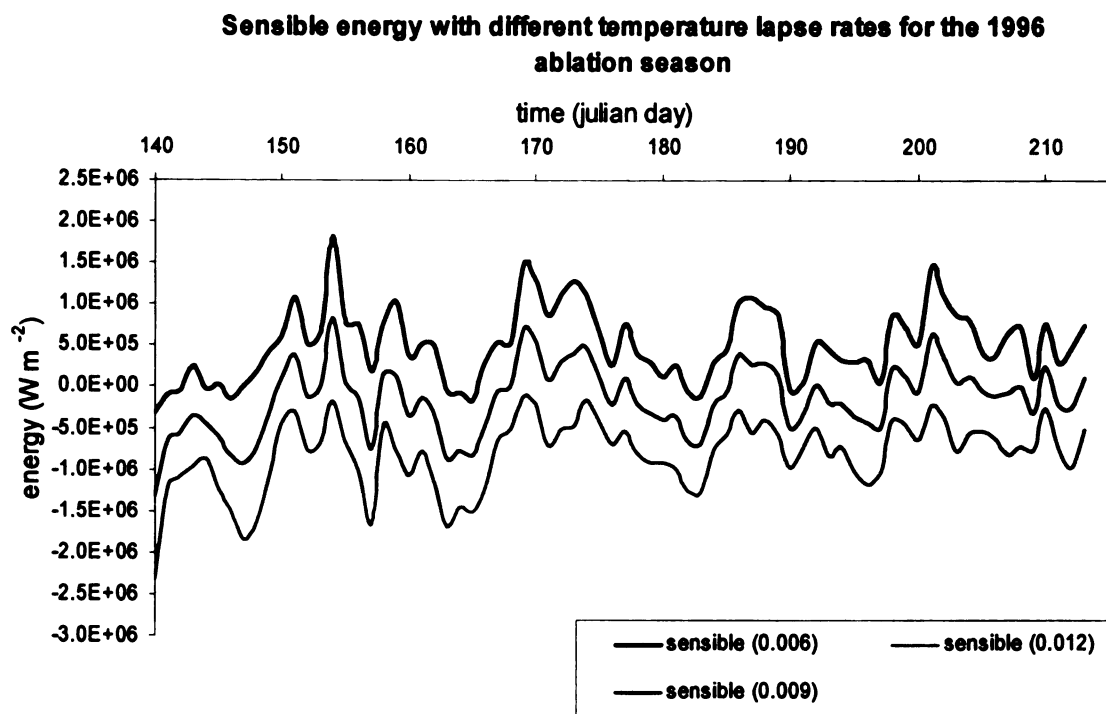


**Figure 9.** *Sensible energy using different temperature lapse rates for the 1996 ablation season.*

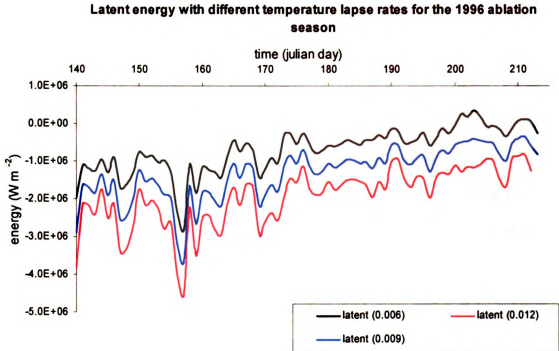


*Figure 10. Latent energy using different temperature lapse rates for the 1996 ablation season*

### **Winter chill layer**

Energy required for heating the glacier winter chill layer to  $0^{\circ}\text{C}$  was calculated for five cells located along the glacier center line from the glacier snout to the accumulation zone for 1996. Energy required ranged from 0.05% of total energy received during the ablation season for the cell at the snout to 0.22% of total energy received during the ablation season for the cell at the accumulation zone. It is the author's opinion that heating up the winter chill layer is not a significant energy sink during the ablation season and accounts for  $< 0.22\%$  of the total energy.

## **Wind speed**

The effect of substituting a wind speed of  $0.01 \text{ m s}^{-1}$  and  $5 \text{ m s}^{-1}$  for that recorded at the glacier weather station on the sensible energy flux is presented in Figure 11. The figure shows that without significant wind the sensible energy flux is very small. On the other hand increasing wind speed to  $5 \text{ m s}^{-1}$  significantly increases the effect of the sensible energy flux, but when comparing it to the total energy flux the effect is minimal.

The effect of substituting a wind speed of  $0.01 \text{ m s}^{-1}$  and  $5 \text{ m s}^{-1}$  for that recorded at the glacier weather station on the latent energy is presented in Figure 12. The figure shows a similar pattern as for the sensible energy flux; without significant wind the latent energy flux is very small, and increasing wind speed to  $5 \text{ m s}^{-1}$  increases the effect of the latent energy significantly. However, compared to the total energy flux the effect is minimal.

It is the author's opinion that wind speed recorded at the glacier weather station is a reasonable input parameter to the surface-energy balance model because it falls within the probable limits of  $0.01 \text{ m s}^{-1}$  and  $5 \text{ m s}^{-1}$ .

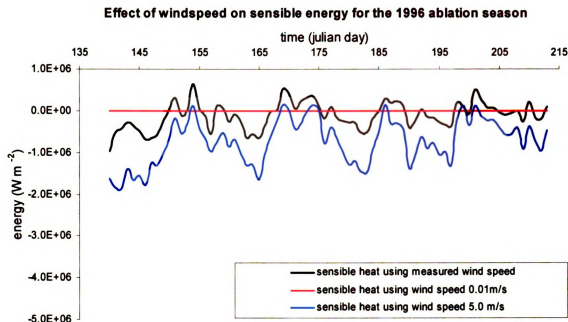


*Figure 11. Effect of substituting measured wind speed with  $0.01 \text{ m s}^{-1}$  and  $5.0 \text{ m s}^{-1}$  on sensible energy for the 1996 ablation season.*

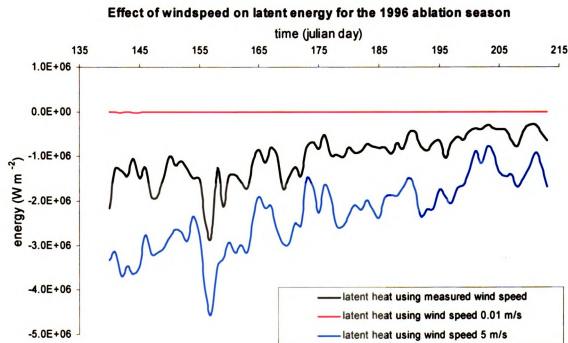


*Figure 12. Effect of substituting measured wind speed with  $0.01 \text{ m s}^{-1}$  and  $5.0 \text{ m s}^{-1}$  on latent energy for the 1996 ablation season.*

## Aerodynamic surface roughness coefficient

The effect of different aerodynamic surface roughness coefficient values on the turbulent energy fluxes for day 140 to day 150 of 1996 is presented in Figure 13. The figure shows that changing the aerodynamic surface roughness coefficient from 0.01m to 0.001m and 0.005m does not significantly change turbulent energy fluxes. It is the author's opinion that a value of 0.01 for the aerodynamic surface roughness coefficient best represents the glacier surface because it is the average of published values (Patterson, 1994).

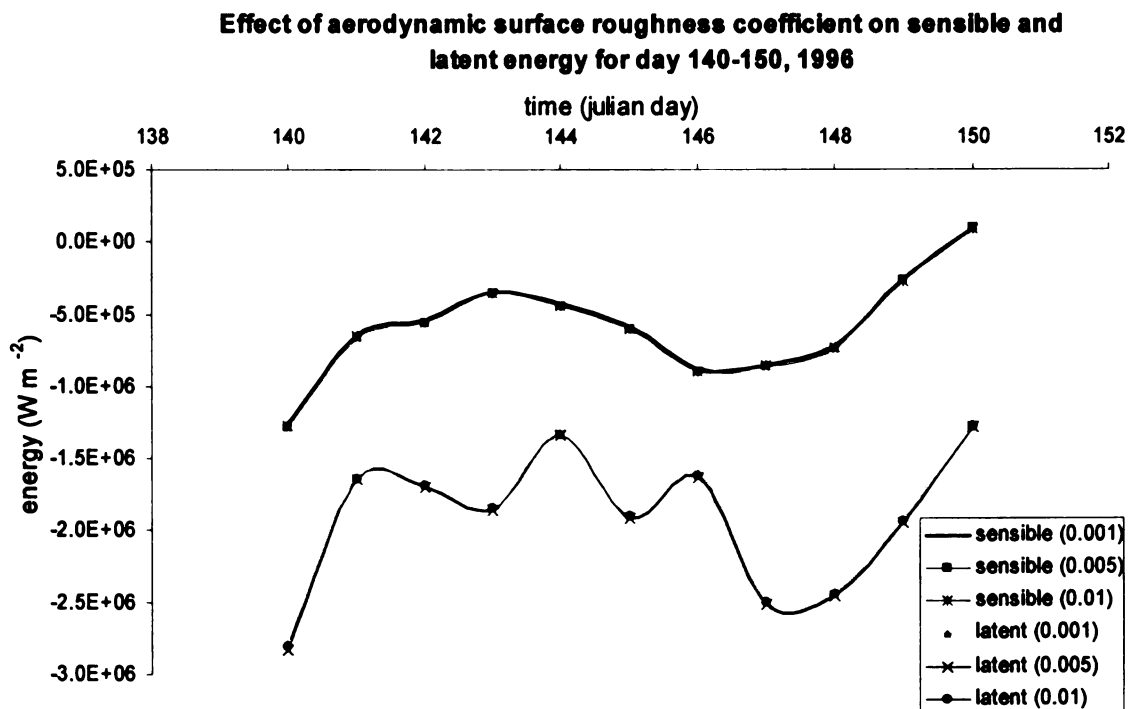


**Figure 13.** *Sensible and latent energy for the Matanuska Glacier with different aerodynamic surface roughness coefficients for day 140 to 150, 1996.*

## Calibration

The surface-energy balance model was calibrated using measured ablation from a point at the snout of the glacier for day 150 to day 213 for 1996. Figure 14 shows that cumulative melt generated using the surface-energy balance model versus cumulative measured ablation is almost similar with an  $r^2$  of 0.9952.

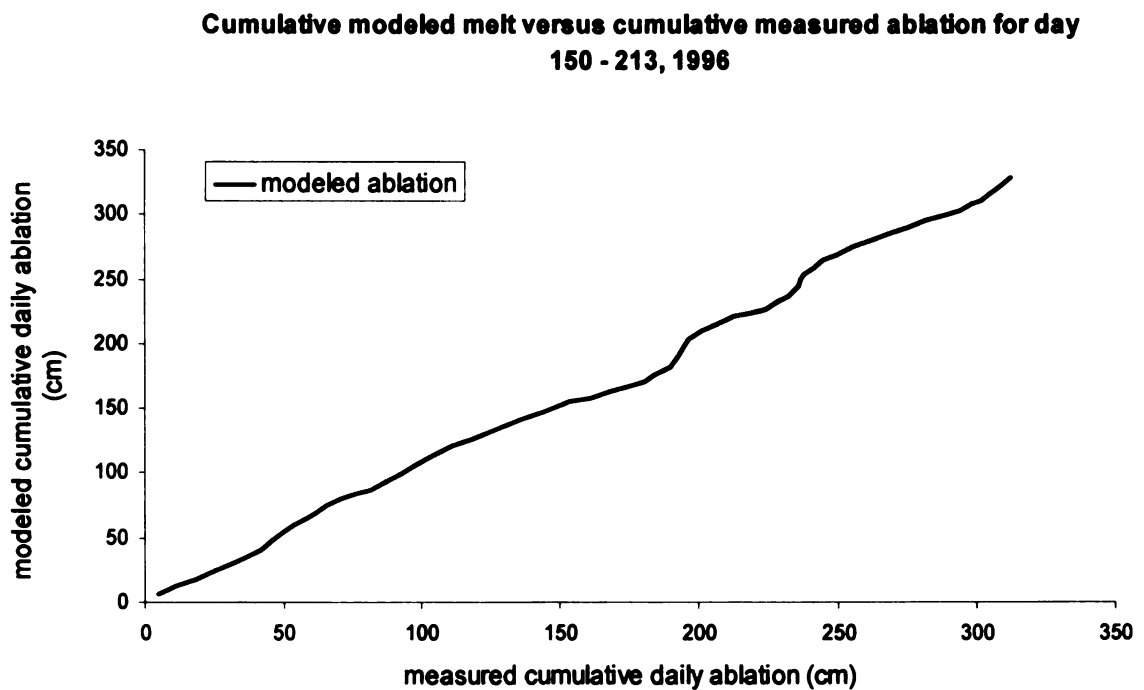


**Figure 14. Cumulative modeled melt versus cumulative measured ablation for day 150 to 213, 1996.**

## RESULTS

### Results for cell at the snout and at the accumulation zone

Figure 15 shows the energy fluxes calculated for two contrasting cells on the glacier surface for day 173 (June 21<sup>st</sup>) of 1996. One of the cells is located at the glacier snout and the other high in the accumulation zone along the center line of the glacier.

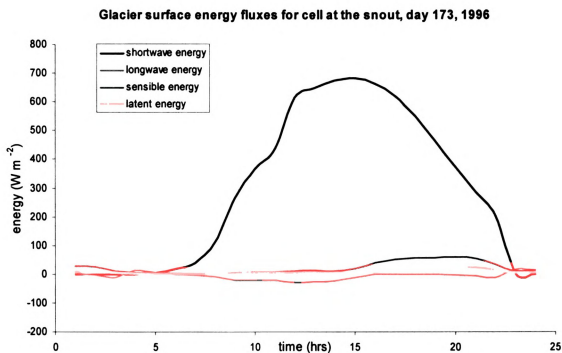


*Figure 15. Shortwave, longwave, sensible and latent energy for a cell at the snout of the glacier at day 173, 1996.*

The figure shows a clear diurnal pattern of shortwave energy flux for the cell at the snout with no shortwave energy before sunrise and almost  $700 W m^{-2}$  around 3 in the afternoon. The longwave energy flux was lowest,  $-30 W m^{-2}$ ,



around noon and sensible and latent energy fluxes were lowest in the morning, increasing to higher fluxes later in the afternoon and early evening. Maximum sensible energy was around  $60 \text{ W m}^{-2}$  and minimum was around  $0 \text{ W m}^{-2}$ ; maximum latent energy was around  $20 \text{ W m}^{-2}$  and minimum around  $0 \text{ W m}^{-2}$ .

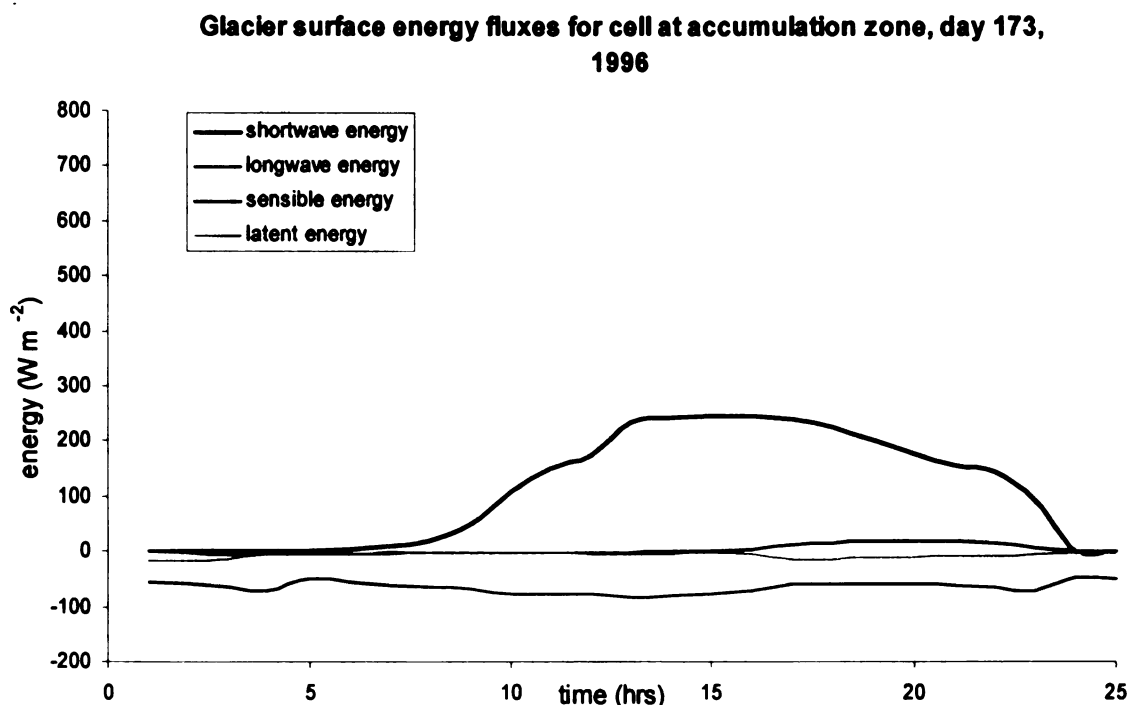


*Figure 16.. Shortwave, longwave, sensible and latent energy for a cell at the accumulation zone of the glacier at day 173, 1996.*

The cell in the accumulation zone showed the same general pattern (Figure 16) for the four fluxes as the cell at the glacier snout. Shortwave energy had a diurnal pattern with the maximum flux around  $300 \text{ W m}^{-2}$ . The longwave energy flux was lowest,  $-80 \text{ W m}^{-2}$  around noon. Sensible energy had lowest values in the night/early morning of around  $-5 \text{ W m}^{-2}$  and increasing to about  $20 \text{ W m}^{-2}$  in the

late afternoon/early evening. Latent energy flux for the cell in the accumulation zone shows a difference with the cell at the snout area. During the day latent energy was fairly stable, just below 0 W m<sup>-2</sup> decreasing to almost -20 W m<sup>-2</sup> in the late afternoon/early evening.

### **Results for entire glacier for 1996 and 1997 ablation seasons**

Results generated from the surface-energy balance model for Julian day 140 to 213 (May 19 to July 31), 1996 and for day 94 to 234 (April 4 to August 22), 1997 are shown in Table 1 and Table 2 and Figure 17 and Figure 18.

*Table 1. Surface-energy balance model results in W m<sup>-2</sup>: average, minimum and maximum shortwave, longwave, sensible and latent energy for day 140 to 213 (May 19 to July 31), 1996.*

	shortwave energy	longwave energy	sensible energy	latent energy	energy for melting
average	1.79E+7	-8.99E+6	-1.31E+5	-1.28E+6	1.27E+7
minimum	8.66E+6	-1.13E+7	-1.26E+6	-3.62E+6	4.88E+6
maximum	2.57E+7	-7.23E+6	8.58E+5	-3.57E+5	2.05E+7

**Table 2.** *Surface-energy balance model results in  $W m^{-2}$ : average, minimum and maximum shortwave, longwave, sensible and latent energy for day 94 to 234 (April 4 to August 22), 1997.*

	shortwave energy	longwave energy	sensible energy	latent energy	energy for melt
average	1.45E+7	-1.04E+7	-6.65E+5	-1.39E+6	9.34E+6
minimum	3.35E+6	-1.79E+7	-4.09E+6	-4.78E+6	7.58E+5
maximum	2.50E+7	-6.73E+6	1.01E+6	4.63E+4	2.14E+7

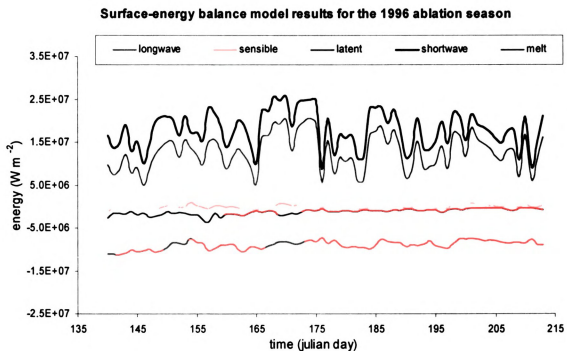


**Figure 17.** *Surface-energy balance model results for the 1996 ablation season.*

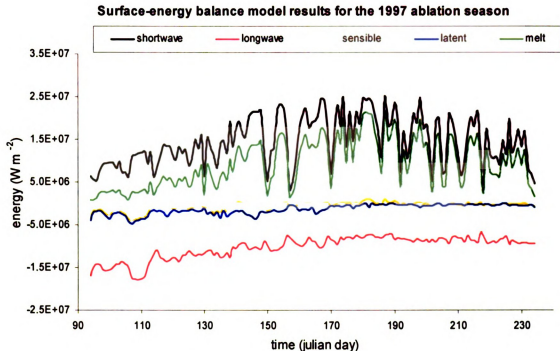


Figure 18. Surface-energy balance model results for the 1997 ablation season.

### Shortwave energy flux

Over the two seasons shortwave energy flux was highly variable. In 1996 values ranged between  $8.66\text{E}+6 \text{ W m}^{-2}$  and  $2.57\text{E}+7 \text{ W m}^{-2}$  with an average flux of  $1.79\text{E}+7 \text{ W m}^{-2}$ . In 1997 values ranged between  $4.88\text{E}+6 \text{ W m}^{-2}$  and  $2.05\text{E}+7 \text{ W m}^{-2}$  with an average flux of  $1.27\text{E}+7 \text{ W m}^{-2}$ . For both 1996 and 1997 the high fluxes reflect a general sinusoidal trend throughout the season with the highest concentrated in the middle of June, when days were longest. Further, the shortwave energy flux was the largest of the four energy fluxes and during most of the period the only positive contributor to energy available for melting ice.

### **Longwave energy flux**

Compared to the shortwave energy flux the longwave energy flux was relatively constant over the modeled periods. In 1996 fluxes ranged between  $-1.13\text{E}+7 \text{ W m}^{-2}$  and  $-7.23\text{E}+6 \text{ W m}^{-2}$  with an average flux of  $-8.99\text{E}+6 \text{ W m}^{-2}$ . In 1997 values ranged between  $-6.73\text{E}+6 \text{ W m}^{-2}$  and  $-1.79\text{E}+6 \text{ W m}^{-2}$  with an average flux of  $-1.04\text{E}+7 \text{ W m}^{-2}$ . For both years a trend of slow increasing longwave energy flux was visible, probably due to increasing air temperatures. The longwave energy flux was the greatest negative energy flux in the energy budget.

### **Sensible energy flux**

The sensible energy flux also did not fluctuate much over the modeled periods. In 1996 sensible energy flux ranged from  $-1.26\text{E}+6 \text{ W m}^{-2}$  to  $8.58\text{E}+5 \text{ W m}^{-2}$ , with an average value of  $-1.31\text{E}+5 \text{ W m}^{-2}$ . In 1997, the sensible energy flux ranged from  $-4.09\text{E}+6 \text{ W m}^{-2}$  to  $1.01\text{E}+6 \text{ W m}^{-2}$  and had an average of  $-6.65\text{E}+5 \text{ W m}^{-2}$ . The lowest flux was early in the season and the highest flux occurred in early June, but the general trend was a slowly increasing flux over the entire period. The sensible energy flux contributed only small amounts to the energy balance, sometimes positive and sometimes negative.

### **Latent energy flux**

Latent energy fluxes in 1996 ranged from  $-3.62\text{E}+6 \text{ W m}^{-2}$  to  $-3.57\text{E}+5 \text{ W m}^{-2}$  with an average of  $-1.28\text{E}+6 \text{ W m}^{-2}$ . In 1997, fluxes ranged from  $-4.78\text{E}+6 \text{ W m}^{-2}$  to  $4.63\text{E}+4 \text{ W m}^{-2}$  with an average flux of  $-1.39\text{E}+6 \text{ W m}^{-2}$ . There was a general trend of slowly increasing flux through the season with some fluctuations early in the ablation period.

### **Total energy flux**

Total energy fluxes in 1996 ranged from  $3.42\text{E}+6 \text{ W m}^{-2}$  to  $1.57\text{E}+7 \text{ W m}^{-2}$  with an average of  $9.85\text{E}+6 \text{ W m}^{-2}$ . In 1997, fluxes ranged from  $7.58\text{E}+5 \text{ W m}^{-2}$  to  $2.14\text{E}+7 \text{ W m}^{-2}$  with an average flux of  $9.34\text{E}+6 \text{ W m}^{-2}$ .

## **DISCUSSION**

### **Modeled melt and measured discharge**

Modeled melt versus measured discharge at the Matanuska Glacier for the 1996 and 1997 ablation seasons are presented in Figure 19 and Figure 20 respectively. The figures show that volumetrically modeled melt and measured discharge do not equal each other and that modeled melt exceeds measured discharge in the early part of the ablation season but that it approaches measured discharge late in the ablation season. Also, the figures show that fluctuations in modeled melt are generally greater than fluctuations in measured discharge throughout the ablation season.

Possible explanations for the discrepancy in volume could include unreliable discharge data, inaccurate glacier weather station data, and errors associated with extrapolation of weather data to cells at higher elevation.

Unreliable discharge may be the result of instrumentation problems; errors associated with rating curves; and/or missed discharge at small non-gauged discharge streams at the northwest margin of the glacier. Even though a discharge accuracy of 93% has been reported by Linker (2001), the author believes inaccuracies related to the North Vent discharge rating curve could result in a significant error in measured discharge. (Discharge for North Vent seems to be far more than the mentioned 6% of total discharge and could in the author's opinion be equal to discharge at South Branch.)

Inaccurate glacier weather data may be the result of instrumentation problems and/or the fact that the weather station is located approximately 200 m from the ice margin and may not accurately record meteorological conditions at the ice surface. It is the author's opinion that this is not an issue, because sensitivity analyses demonstrated that a 2°C change in temperature and substitution of 0 and 5 m s<sup>-1</sup> for wind speed leads to no significant change in total melt. Also, measured incoming solar energy values are consistent with measured values from nearby weather stations located in Anchorage, Talkeetna and Gulkana, Alaska (Ross, 1999).

Errors due to extrapolation of weather data to cells on the glacier at higher elevation may be the result of applying an incorrect lapse rate, a possibility created by katabatic conditions occurring along the glacier's length. Despite the fact that the surface-energy balance model is correctly representing melt for a point near the snout of the glacier it may not be correctly representing melt for points at higher elevations. Sensitivity analyses showed substituting the temperature lapse rate by 0.006°C m<sup>-1</sup> and 0.012°C m<sup>-1</sup> does not appreciably affect the total energy balance of the glacier surface.

Modeled melt for the 1996 (Figure 19) and 1997 (Figure 20) ablation seasons shows low frequency fluctuations superimposed on generally consistent values throughout the ablation season. On the other hand, measured discharge shows low frequency fluctuations superimposed on low values during the early part of the ablation season and low frequency fluctuations superimposed on generally high values during the later part. An explanation for the difference in



discharge is that melt at the beginning of the ablation season is temporarily stored in the glacier, especially in seasonal snow cover. However, later in the ablation season modeled melt corresponds more closely with measured discharge because the storage capacity of the glacier has been reached, the seasonal snow cover has melted and a more developed drainage network has evolved. During the later part of the ablation season peaks in modeled melt generally coincide with peaks in measured discharge and sometimes precede or follow peaks in measured discharge by a few days.

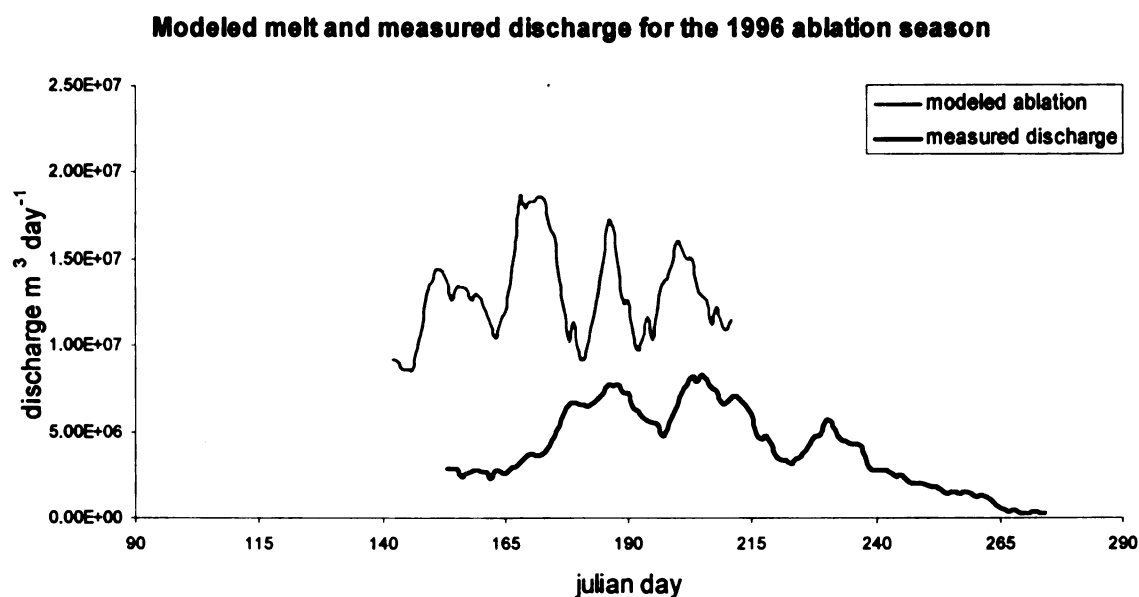


*Figure 19. Modeled melt and measured discharge for the 1996 ablation season.*

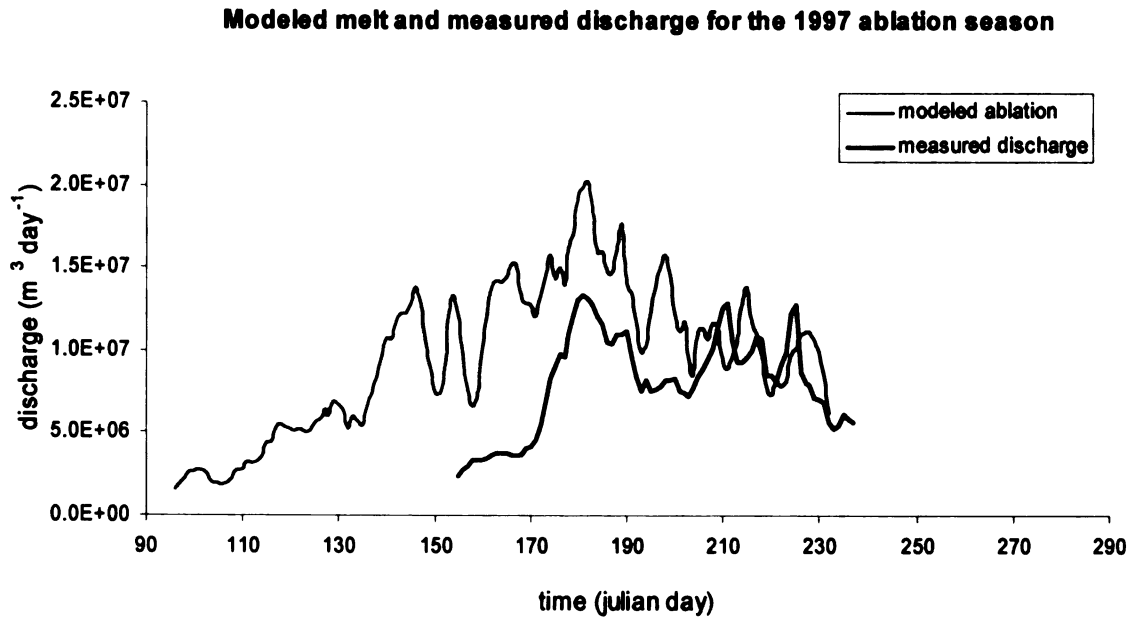


*Figure 20. Modeled melt and measured discharge for the 1997 ablation season.*

### **Measured discharge and ice-surface velocity**

Early in the 1996 and 1997 ablation seasons measured discharge and ice-surface velocity show different trends (Figure 21 and 22). Measured discharge is characterized by low frequency fluctuations superimposed on low discharge values during the early part of the ablation season and by low frequency fluctuations superimposed on generally high discharge values during the later part. In contrast, ice-surface velocity is characterized by high frequency fluctuations superimposed on fairly consistent values throughout the entire ablation season. During most part of the 1996 and 1997 ablation seasons peaks in measured discharge generally coincide or precede by a few days drops in ice-surface velocity. According to Ensminger et al. (1999) this is due to the evolution and configuration of the drainage system and storage of meltwater in the glacier.

A notable exception to this is late in the 1997 ablation season (after day 228) , when measured discharge decreases below  $6.0\text{E}+6 \text{ m}^3 \text{ day}^{-1}$  , while ice-surface velocity increases to a maximum of  $25 \text{ cm day}^{-1}$  . An explanation for this could be localized blockage of conduits by glaciohydraulic supercooling and freeze-on at the bed of the glacier, a process widely described at the Matanuska Glacier (Lawson et al. 1998a, b; Larson et al., 2006).

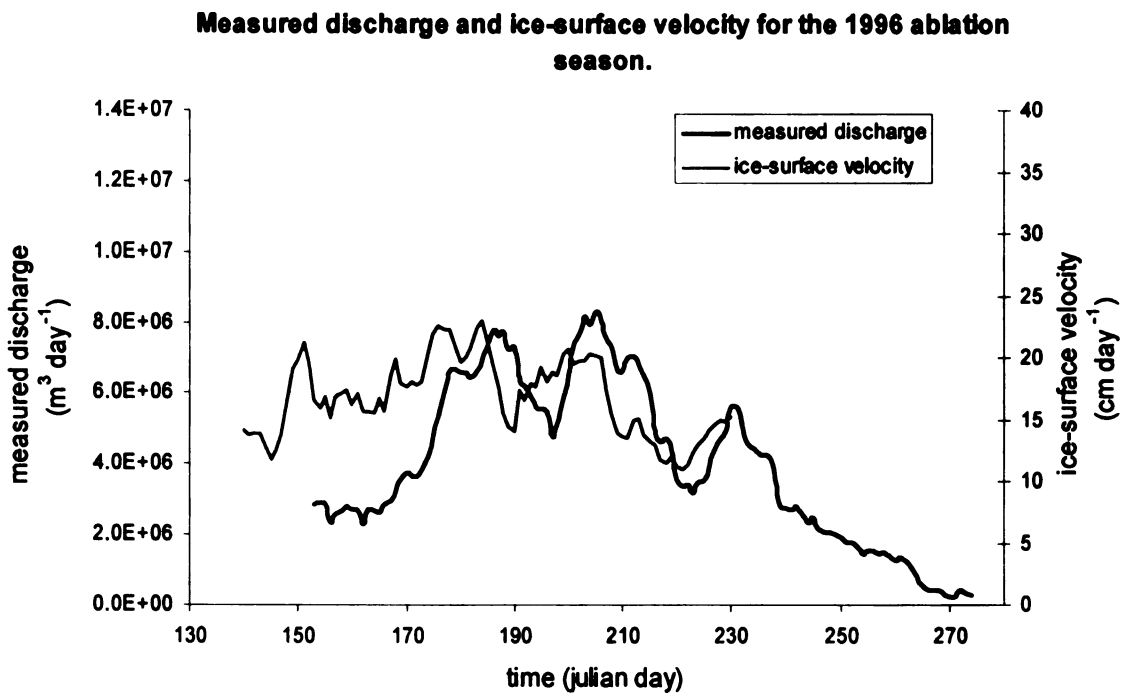


**Figure 21. Measured discharge and ice-surface velocity for the 1996 ablation season.**

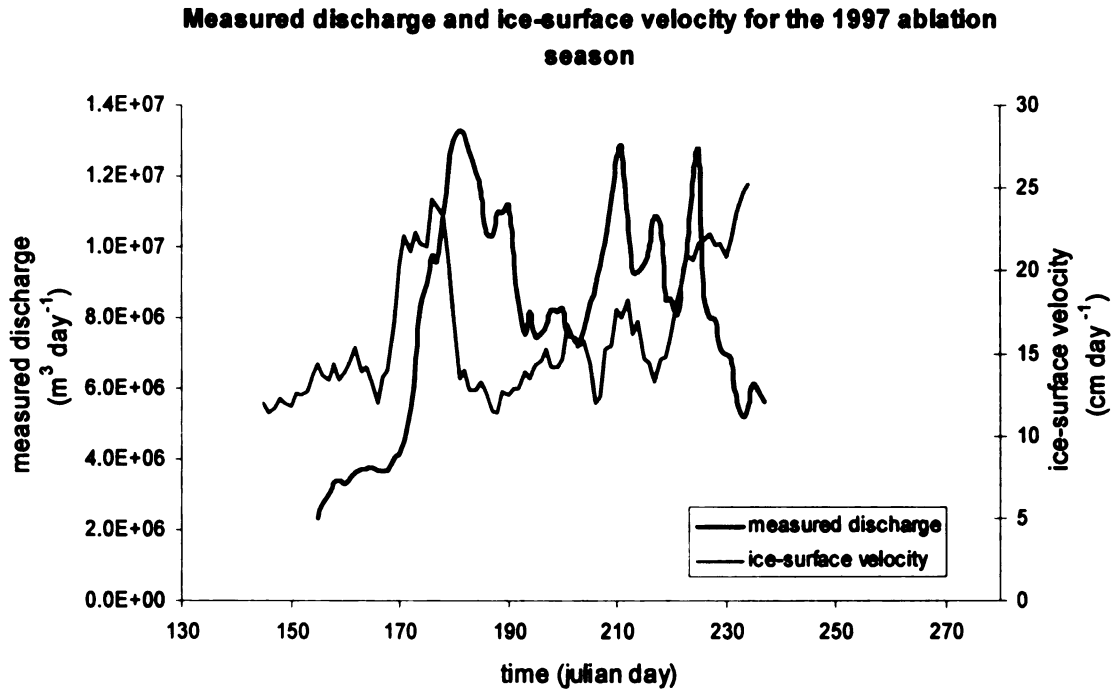


*Figure 22. Measured discharge and ice-surface velocity for the 1997 ablation season.*

### **Meltwater storage and ice-surface velocity**

Figure 23 and Figure 24 show the relationship between meltwater storage and ice-surface velocity for the 1996 and 1997 ablation seasons. Despite the fact that values of modeled melt and measured discharge for 1996 and 1997 are not in balance, the figure still shows trends between meltwater storage and ice-surface velocity. For example, between Julian day 165 and 185 of the 1996 and 1997 ablation seasons meltwater storage reaches its highest peak and is followed 2 to 4 days later by a high peak in ice-surface velocity. This relationship confirms several studies (Iken, 1981; Iken et al., 1983; Hooke et al, 1985; Iken

and Bindshadler, 1986; Iken and Truffer, 1997; Ensminger et al, 1999; Jansson et al, 2003) suggesting a direct relationship between meltwater storage and ice-surface velocity.

Lliboutry (1968), Kamb(1970), Iken et al. (1983), Hooke et al. (1989), Ensminger (1999) and Jansson et al. (2003) have suggested that an explanation for the increase in ice-surface velocity following increase in meltwater storage is due to temporarily storage of meltwater in the early ablation season in an undeveloped distributed subglacial drainage network decoupling the glacier from its bed and decreasing friction at the bed. Eventually, ice-surface velocity decreases as a more developed network of subglacial channels forms at the glacier bed, temporarily stored meltwater is discharged, resulting in lowering the glacier back on to its bed and increasing friction at the glacier bed.

Peaks of high ice-surface velocity also occur other than from day 165 to 185. For example, one occurs during day 147 to 154 of 1996. The explanation for this peak could be related to increased meltwater storage, but cannot be tested because of lack of glacier weather station and discharge data for this period. Another peak in ice-surface velocity occurs from day 191 to day 208 of 1996. The explanation for this peak could be the result of peak in meltwater storage around day 187. Between days 194 and 217 a couple of small peaks (around days 202 and 212) in ice-surface velocity occur that may be related to small preceding storage peaks, but available data does not show a well developed relationship between meltwater storage and ice-surface velocity for this period. A possible explanation for this could be that as the ablation season progresses the

distributed drainage system at the bed of the glacier evolves into a network of channels, minimizing frictional fluctuations at the glacier bed and resulting in a reduced relationship between meltwater storage and ice-surface velocity (Lliboutry, 1968; Kamb, 1970; Iken et al., 1983; Hooke et al., 1989; Ensminger et al., 1999; and Jansson et al., 2003). After day 220 of 1997 ice-surface velocity increases to a high of  $25 \text{ cm s}^{-1}$  not preceded by high meltwater storage. An explanation for this is not understood, but may be due to restriction of subglacial channels by basal freeze-on mechanisms (Hooke and Pohjola, 1994; Lawson et al., 1998a, b, and Larson, 2006) resulting in localized increased water pressure in the channels and lifting of the glacier from its bed.

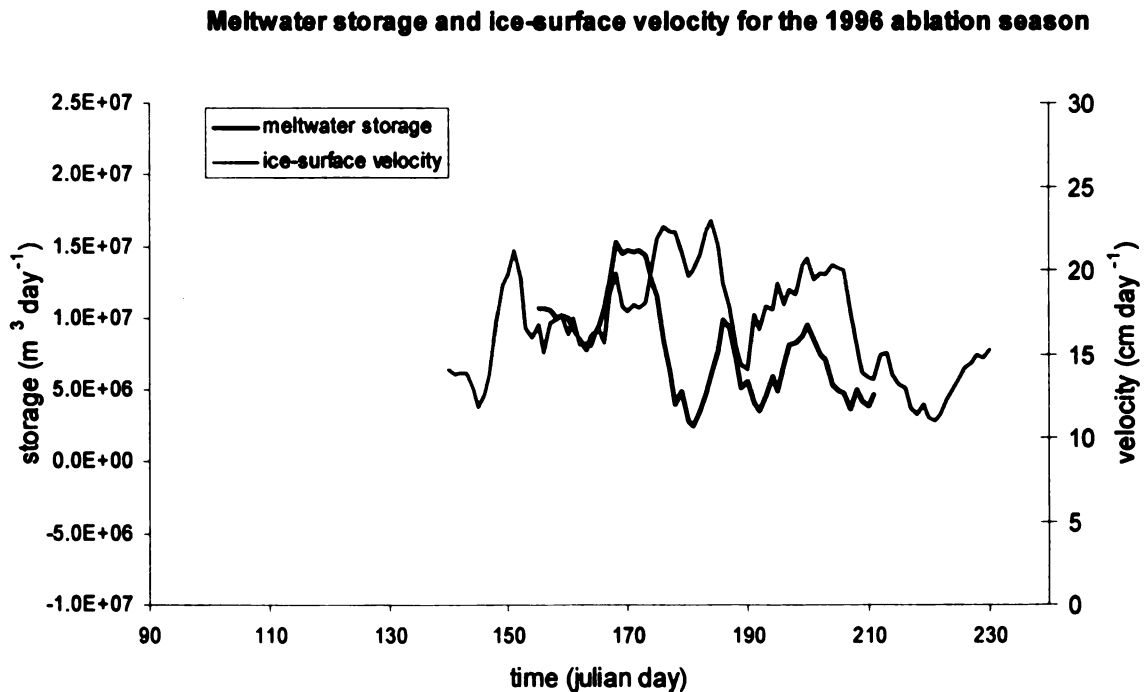


**Figure 23. Meltwater storage and ice-surface velocity for the 1996 ablation season.**

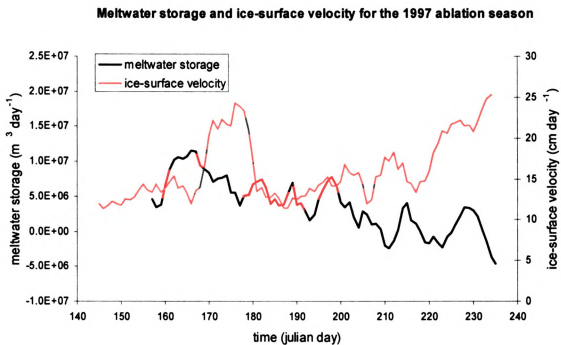


*Figure 24. Meltwater storage and ice-surface velocity for the 1997 ablation season.*

## **CONCLUSIONS**

Modeled melt at the Matanuska Glacier for the 1996 and 1997 ablation seasons shows the following:

- Shortwave energy is positive and contributes the most to the energy balance at the glacier surface.
- Longwave, sensible and latent energy are mostly negative and contribute little to the glacier energy balance, with longwave energy being most negative.
- Shortwave energy becomes smaller at higher elevations due to increasing albedo. Longwave energy becomes increasingly more negative at higher elevations due to decreasing temperatures. Changes in sensible and latent energy are minimal.
- Increasing air temperatures by 2°C, substituting wind speed by 0.01 m s<sup>-1</sup> and 5.0 m s<sup>-1</sup> and substituting surface roughness coefficient by 0.001m and 0.005m and substituting temperature lapse rate by 0.006°C m<sup>-1</sup> and 0.012°C m<sup>-1</sup> does not appreciably affect the total energy balance
- Heating the winter chill layer does not act as a significant energy sink during the ablation season
- Shadow of surrounding topography only accounts for a 7% decrease in the surface-energy balance

Analyses of modeled melt, measured discharge, ice-surface velocity and meltwater storage for the 1996 and 1997 ablation seasons shows the following:



- Modeled melt has generally consistent values throughout the ablation season. Measured discharge is generally low early in the ablation season and generally high in the later part.
- Later in the ablation season peaks in modeled melt generally coincide and sometimes precede or follow peaks in measured discharge by a few days.
- During most of the ablation season peaks in measured discharge generally coincide or are preceded by a few days by decreasing ice-surface velocity.
- A change in meltwater storage in the early part of the ablation season results in a change in ice-surface velocity.
- Later in the ablation season there is not an obvious relationship between meltwater storage and ice-surface velocity.

### **General conclusion**

The surface-energy balance of the Matanuska Glacier is most sensitive to changes in solar radiation and only moderately to changes in air temperature. Because of this the Matanuska Glacier margin has been relatively stable over the last 200 hundred years compared to glaciers sensitive to air temperature fluctuations.

## REFERENCES

- Andreas, E. L., 1987, A theory for the scalar roughness and the scalar transfer coefficients over snow and sea ice. *Boundary-Layer Meteorology*, 38, 159-184.
- Arnold, N. S., Willis, I. C., Sharp, M. J., Richards, K. S., Lawson, W. J., 1996. A distributed surface energy-balance model for a small valley glacier. I. Development and testing for the Haut Glacier d'Arolla, Valais, Switzerland. *Journal of Glaciology*, 42, 77-89.
- Braithwaite, R. J., 1995, Aerodynamic stability and turbulent sensible-heat flux over a melting ice surface, the Greenland Ice Sheet. *Journal of Glaciology*, 36, 222-228.
- Braithwaite, R. J., Olesen, O. B., 1990, A simple energy-balance model to calculate ice ablation at the margin of the Greenland Ice Sheet. *Journal of Glaciology*, 36, 222-228.
- Brock, B., W. and Arnold, N. S., 2000, A spreadsheet-based (Microsoft Excel) point surface energy balance model for glacier and snow melt studies. *Earth Surface Processes and Landforms*, 25, 649-658.
- Ensminger, S. L., Evenson, E. B., Alley, R. B., Larson, G. L., Lawson, D. E., Strasser, J. C., 1999, Example of the dependence of ice motion on subglacial drainage system evolution: Matanuska Glacier, Alaska, United States, in Mickelson, D. M., and Attig, J. W., eds., *Glacial Processes Past and Present*: Boulder, Colorado, Geological Society of America Special Paper 337.
- Hannah, D. M., Gurnell, A. M., and McGregor, G. R., 1999, Spatio-temporal variation in microclimate, the surface energy balance and ablation over a cirque glacier. *International Journal of Climatology*, 20, 733-758.
- Harper, J. T., Humphrey, N. F., Pfeffer, W.T., Fudge, T., and O'Neel, S., 2005, Evolution of subglacial water pressure along a glacier's length. *Annals of Glaciology*, 40, 1-6.
- Hodgkins, R., 2001, Seasonal evolution of melt water generation, storage and discharge at a non-temperate glacier in Svalbard: *Hydrological Processes*, 15, p. 441-460.

- Hock, R. and Holmgren, B., 2005, A distributed surface energy-balance model for complex topography and its application to Storglaciären, Sweden. *Journal of Glaciology*, 51, 25-36.
- Hock, R. and Noetzli, C., 1997, Areal melt and discharge modeling of Storglaciären, Sweden. *Annals of Glaciology*, 24, p. 211-216.
- Hooke, R. L., Wold, B., and Ove Hagen, J., 1985, Subglacial hydrology and sediment transport at Bondhusbreen, southwest Norway. *Geological Society of America Bulletin*, 96, p. 388-397.
- Hooke, R. L., Calla, P., Holmlund, P., Nilsson, M., and Stroeven, A., 1989, A 3 year record of seasonal variations in surface velocity, Storglaciären, Sweden. *Journal of Glaciology*, 35, p. 235-247.
- Hooke, R. LeB. And Pohjola, V. A., 1994, Hydrology of a segment of a glacier situated in an overdeepening, Storglaciären, Sweden. *Journal of Glaciology*, 40, 140-148.
- Iken, A., 1981, The effect of the subglacial water pressure on the sliding velocity of a glacier in an idealized numerical model: *Journal of Glaciology*, 27, p. 407-421.
- Iken, A., Röthlisberger, H., Flotron, A., and Haeberli, W., 1983, The uplift of Unteraargletscher at the beginning of the melt season. A consequence of water storage at the bed? *Journal of Glaciology*, 29, 28-47.
- Iken, A., Bindschadler, R.A., 1986, Combined measurements of subglacial water pressure and surface velocity of Findelengletscher, Switzerland: conclusions about drainage system and sliding mechanism. *Journal of Glaciology*, 32, 101-119.
- Iken, A., and Truffer, M., 1997, The relationship between subglacial water pressure and surface velocity of Findelengletscher, Switzerland, during its advance and retreat. *Journal of Glaciology*, 43, 328-338.
- Inoue, J., 1989, Surface drag over the snow surface of the Antarctic Plateau. I. Factors controlling surface drag over the katabatic wind region. *Journal of Geophysical Research*, 94, 2207-2218.
- Jansson, P., Hock, R., Schneider, T., 2003, The concept of glacier storage: a review. *Journal of Hydrology*, 282, 116-129.
- Kamb, B., 1970, Sliding motion of glaciers: Theory and observation. *Reviews of Geophysics and Space Physics*, 8, p. 673-729.

- Larson, G.L., Lawson, D. E., Evenson, E. B., Alley, R. B., Knudsen, O., Lachniet, M. S., and Goetz, S. L., 2006, Glaciohydraulic supercooling in former ice sheets? *Geomorphology*, 75, 20-32.
- Lawson, D. E., Evenson, E. B., Larson, G. L., Alley, R. B., 1998a, Glacier dynamics, sediment entrainment, transport and deposition, and hummocky moraine genesis. AGU Annual Fall Meeting, San Fransisco, EOS Transactions, 79, pp. F726.
- Lawson, D. E., Strasser, J. C., Evenson, E. B., Alley, R. B., Larson, G. L., and Arcone, S. A., 1998b, Glaciohydraulic supercooling: a freeze-on mechanism to create stratified, debris-rich basal ice. 1. Field evidence. *Journal of Glaciology*, 44, 547-562.
- Liboutry, L., 1968, General theory of subglacial cavitation and sliding of temperate glaciers. *Journal of Glaciology*, 7, p. 21.
- Linker, J. S., 2001 Sediment flux as an indicator of glacial erosion Matanuska Glacier, Alaska. *Master Thesis*, Department of Geological Sciences. Michigan State University, East Lansing, 49.
- Matsumoto, T., Naruse, R., Konya, K., Yamaguchi, S., Yamada, T., and Muravyev, Y. D., 2004, Summer water balance characteristics of Koryto Glacier, Kamchatka Peninsula, Russia. *Geografiska Annaler*, 86A, p. 181-190.
- Munro, D. S., 1989, Surface roughness and bulk heat transfer on a glacier: comparison with eddy correlation. *Journal of Glaciology*, 35, 343-348.
- Munro, D. S., 1990, Comparison of melt energy computations and ablatometer measurements on melting ice and snow. *Arctic and Alpine Research*, 22, 153-162.
- Naruse, R., Fukami, H., and Aniya, M., 1992, Short-term variations in flow velocity of Glacier Soler, Patagonia, Chile. *Journal of Glaciology*, 38, 152-156.
- Obukhov, A. M., 1971, Turbulence in an atmosphere with a non-uniform temperature. *Boundary-Layer Meteorology*, 2, 7-29
- Oke, T. R., 1987, *Boundary layer climates*, second edition Methuen: London, 450 pp.
- Paterson, W. S. B., 1994, *The physics of glaciers*: New York, Pergamon Press, 480 pp.

- Raymond, C.F., Benedict, R.J., Harrison, W.D., Echelmeyer, K.A., and Sturm, M., 1995, Hydrological discharges and motion of Fels and Black Rapid Glaciers, Alaska, USA: implications for the structure of their drainage systems. *Journal of Glaciology*, 41, 290–304.
- Ross, T., compiler. 1999, National Solar Radiation Data Base hourly solar data from Alaska, 1961-1990. Boulder, CO: National Snow and Ice Data Center. Digital media.
- Schuler, T., Fischer, U.H., Sterr, R., Gudmondsson, G.H., Hock, R., 2002, Comparison between modeled water input and measured discharge prior to a release event: Unteraargletscher, Bernese Alps, Switzerland. *Nordic Hydrology*, 33, 27-46.
- Singh, P., Haritashya, U. K., and Kumar, N., 2003, Seasonal changes in meltwater storage and drainage characteristics of the Dokriani Glacier, Garhwal Himalayas (India). *Nordic Hydrology*, 35, p. 15–29.
- Stull, R. B., 1988, *An introduction to Boundary Layer Meteorology*: Dordrecht, Kluwer, 684 pp.
- Tangborn, W., 1999, A mass balance model that uses low-altitude meteorological observations and the area–altitude distribution of a glacier. *Geografiska Annaler: Series A, Physical Geography*, 81, 753-765.
- Waterson, N. J., 2003, Subglacial erosion and the fate of coarse material in the subglacial drainage system of the Matanuska Glacier, Alaska. *Master Thesis*, Department of Geological Sciences. Michigan State University, East Lansing, 44.
- Williams, J. R., and Ferrins, O. J., Jr., 1961, Late Wisconsin and recent history of the Matanuska Glacier, Alaska. *Arctic*, 14, 82-90.
- Willis, I. C., Sharp, M. J. and Richards, K. S., 1992, Studies of the water balance of Midtdalsbreen, Hardangerjøkulen, Norway. II. Water storage and runoff prediction: *Zeitschrift für Gletscherkunde und Glazialgeologie*, v. 27/28, p. 117-138.
- Yamaguchi, S., Naruse, R., Matsumoto, T. and Ohno, H., 2003, Multiday Variations in Flow Velocity at Glaciar Soler, Northern Patagonia, Chile: *Arctic, Antarctic, and Alpine Research*, 35, p. 170–174.
- Western Regional Climate Center, <http://www.wrcc.dri.edu>.